ACS APPLIED MATERIALS & INTERFACES

www.acsami.org

Research Article

Clathrating CO_2 in a Supramolecular Granatohedron Cage with Noncovalent CO_2–NH_3 Interactions and High CO_2 Capture Efficiency under Ambient Conditions

Xiao Lu, Congyan Liu, Xin Xiao, Thien S. Nguyen, Zhiling Xiang, Chunhui Chen, Songlin Cui, Cafer. T. Yavuz,* Qiang Xu,* and Bo Liu*

Cite This: *ACS Appl. Mater. Interfaces* 2023, 15, 54458–54465

Read Online

ACCESS | Metrics & More | Article Recommendations | Supporting Information

ABSTRACT: Organic amine (R–NH_2) reagents as dominant chemical sorbents for CO_2 capture in industrial processes suffer from high energy compensation for regeneration. Herein, we, for the first time, report the finding of Co(III) coordinating with NH_3 molecules regulating the interaction between NH_3 and CO_2 to electrostatic interactions instead of a chemical reaction and achieve CO_2 capture under near-ambient conditions. NH_3 coordinating with Co(III) significantly reduces its alkalinity and reactivity with CO_2 owing to its lone-pair electron donation during coordination. Under a simple protocol, CO_2 induces the crystallization of CO_2@$[Co(NH_3)_6]$-$[HSO_4][SO_4]$ clathrate into a hydrogen-bonded granatohedron cage from a cobaltic hexammine sulfate aqueous solution under a CO_2 pressure of 56 and 142 kPa at 275 and 298 K, respectively, with a CO_2 uptake weight content of 11.7%. We reveal that CO_2 interacts with cobaltous hexammine via supramolecular interactions rather than chemical bonding. The clathrate spontaneously separates from the solution as single crystals and readily releases CO_2 under ambient conditions in water for cyclic utilization without further treatment. In such a rapid supramolecular capture process, molecular recognition ensures exclusive CO_2 selectivity, and soluble clathrate enables the spontaneous CO_2 release at a low energy penalty, exhibiting excellent practical potential in carbon capture.

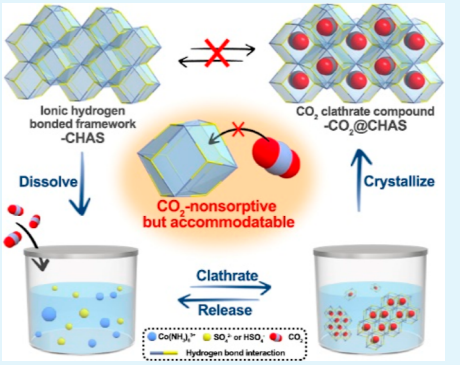

KEYWORDS: *cobaltic hexammine, hydrogen-bonded cage, supramolecular carbon capture, electrostatic interaction, CO_2 clathrate*

INTRODUCTION

The combustion of fossil fuels releases greenhouse gas CO_2, leading to a steady increase in global temperatures.[1] Reducing carbon emissions and enhancing carbon capture are essential to address global warming. A scalable carbon capture technology is needed for practical reasons, as excess global CO_2 emissions are at around 44 billion tons per year.[2] With these in mind, CO_2 sorbents need to meet the following general requirements: exclusive selectivity, low regeneration energy, high adsorption amount in both mass and volume percentages, low cost and easy preparation of the raw materials, fast sorption kinetics, and long durability and stability.[3] Intensive research has been devoted to develop new carbon capture reagents and techniques, including ionic liquids, cryogenic ethanol, membranes, and porous materials,[4] where each technique possesses its own advantages and shortcomings. Although these new technologies show promise for carbon capture, they are still far from the standards of industrial-scale applications.

To date, CO_2 capture technology at the industrial scale is still based on sorption with aqueous amines such as monoethanolamine (MEA), which was proposed by Bottoms in the 1930s.[5] In a MEA-based carbon capture process, the reaction between CO_2 and MEA forms a mixture of carbamates and carbonates so that the regeneration of MEA from aqueous solution requires a temperature higher than 100 °C for MEA recovery because of the water evaporation and thus high energy consumption. Other organic amines (R–NH_2) have also been widely explored for carbon capture, usually via tethering on the inner surface of porous materials to strengthen the CO_2 interaction with sorbents.[6] Organic guanidine with the general formula R–NH–$C(NH_2)_2$ has been reported as a carbon capture agent, as its aqueous solution can directly adsorb CO_2 from air at low partial pressure and be converted to guanidinium carbonate in the form of crystals for automatic separation.[7] Nevertheless, guanidine regeneration requires temperatures above 120 °C for removal of lattice water and guanidinium carbonate decomposition.[8] Ammonia solution, as a CO_2 capture sorbent,

Received: August 13, 2023
Revised: October 19, 2023
Accepted: November 3, 2023
Published: November 16, 2023

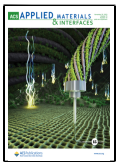

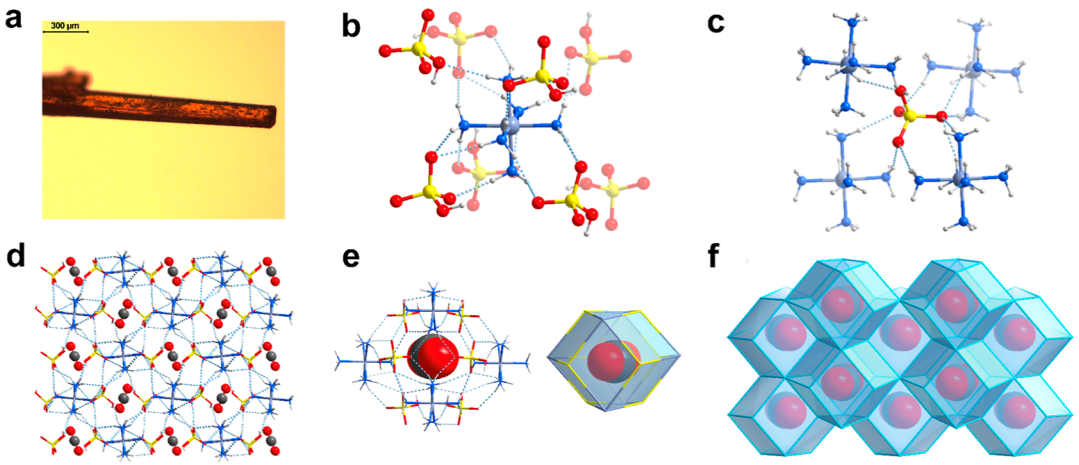

Figure 1. Crystal structure of CO_2@CHAS. (a) Optical picture of the CO_2@CHAS crystal. (b) $[Co(NH_3)_6]^{3+}$ ion contacting eight neighboring HSO_4^-/SO_4^{2-} ions via H-bonds. (c) HSO_4^-/SO_4^{2-} ion connecting with four adjacent $[Co(NH_3)_6]^{3+}$ ions via H-bonds. (d) Three-dimensional (3D) hydrogen-bonded framework of CO_2@$[Co(NH_3)_6][HSO_4][SO_4]$. (e) CO_2 molecule confined in the hydrogen-bonded networking and the corresponding simplified granatohedron cage by connecting adjacent S and Co atoms. (f) Granatohedron cages stacking into a 3D network with a disordered flu topological structure. Color codes: red, oxygen; yellow, sulfur; white, hydrogen; blue, nitrogen; dusty blue, cobalt; and dark gray, carbon (all figures in this article follow this color code).

benefits from its high adsorption capacity and low regeneration energy but suffers from the high volatility of ammonia; hence, its practical application is restricted.[9−14] Aqueous solutions of NaOH, KOH, and $Ca(OH)_2$ as CO_2 sorbents form carbonates with ultrahigh decomposition temperatures at 800−900 °C, making cycling difficult and inefficient.[15−19] Although the physical adsorption of CO_2 using highly porous materials shows great promise and advances, moisture interference and poor CO_2 selectivity restrict its application in industry.[20]

Reactions of CO_2 with different types of amines are summarized in Scheme S1. In general, chemical adsorption using such amine (base) aqueous solutions possesses advantages such as a high absorption capacity and applicability at low CO_2 partial pressures. However, sorbent regeneration requires intensive energy input. Therefore, it is essential to lower the interaction between amines and CO_2 to recover the amines more easily for energy-efficient cycling utilization. Owing to the strong basic nature of NH_3 and organic amines in aqueous solution, they react with CO_2 to afford the formation of ammonium and HCO_3^-/CO_3^{2-}. The alkalinity and the resulting reactivity of NH_3 originate from the lone-pair electrons on the nitrogen atom. In our previous work, we have demonstrated the CO_2-induced formation of single-crystalline carbon dioxide clathrate (CO_2@Gua_2SO_4, Gua = guanidinium) under mild conditions and revealed that the amino groups interact with CO_2 via electrostatic interactions instead of chemical bonds owing to the delocalization of lone-pair electrons from amino groups to carbocations of guanidinium ions.[21] Accordingly, we propose that NH_3 coordination via the donation of its lone-pair electrons to the empty orbital of the transition metal will greatly reduce its alkalinity and reactivity. Herein, we report the finding that ammonia coordinating with Co^{3+} from $CoSO_4/H_2O_2/H_2SO_4$ (concentrated) aqueous solution leads to the formation of $[Co(NH_3)_6][HSO_4][SO_4]$ (cobaltic hexamine sulfate, denoted as CHAS), and we further demonstrate that CO_2 exposure to CHAS solution results in the precipitation of CO_2@CHAS clathrates as single crystals. Impressively, the formation and decomposition of the clathrate, accompanied by CO_2 capture and release, are achieved under near-ambient conditions with remarkable CO_2 uptake capability, exclusive CO_2 selectivity, and low regeneration energy penalty, exhibiting great potential for an industrial-scale application. The CO_2@CHAS is thermally more stable than our first clathrate, CO_2@Gua_2SO_4, enabling a more robust industrial use.

RESULTS

Crystal Structure of CHAS and CO_2@CHAS. Single crystals of CHAS were synthesized from a mixture of $CoSO_4$, H_2O_2, and concentrated H_2SO_4 at 80 °C, and the crystal structure was determined by a single-crystal X-ray diffraction (SCXRD) experiment (Figures S1−S3 and Tables S1 and S2). The oxidation state of cobalt is confirmed to be trivalent by X-ray photoelectron spectroscopy (XPS) (Figure S1b) owing to the presence of the strong oxidants H_2O_2 and concentrated H_2SO_4. Accordingly, two sulfates are assigned to $[HSO_4]^-$ and $[SO_4]^{2-}$ for overall electric neutrality, and the H occupancy on each sulfate is determined to be 50% in crystallography. Other attempts using divalent metal ions, such as Zn^{2+}, Cu^{2+}, Co^{2+}, Fe^{2+}, and Ni^{2+}, failed to isolate stable salts comprising NH_3-coordinated cations under similar conditions but without adding H_2O_2. This is explained by the more positive Co^{3+} ion having a higher affinity with NH_3 for $[Co(NH_3)_6]^{3+}$ formation, which has been reported for catalytic applications previously.[22] In CHAS, $[Co(NH_3)_6]^{3+}$ adopts a regular octahedron configuration, stacking together with HSO_4^-/SO_4^{2-} ions via multiple hydrogen bonds and electrostatic interactions. Taking $[Co(NH_3)_6]^{3+}$ and HSO_4^-/SO_4^{2-} as nodes, a disordered flu topological structure can be depicted, which contains irregular hydrogen-bonded granatohedron cages bearing a closed opening with a diameter of 3.4 Å (Figures S2 and S3, Table S2). The N_2 and CO_2 sorption isotherms are collected at 77 and 273 K over CHAS, respectively, suggesting that the cages are inaccessible toward both N_2 and CO_2 molecules (Figure S4).

When charging the CHAS aqueous solution with CO_2 (see experimental details in Supporting Information), reddish-orange single crystals of CO_2@CHAS are obtained (Figures 1a and S5). The crystal structure of CO_2@CHAS was determined by SCXRD at 100 K (Table S1). CO_2@CHAS

https://doi.org/10.1021/acsami.3c11994
ACS Appl. Mater. Interfaces 2023, 15, 54458−54465

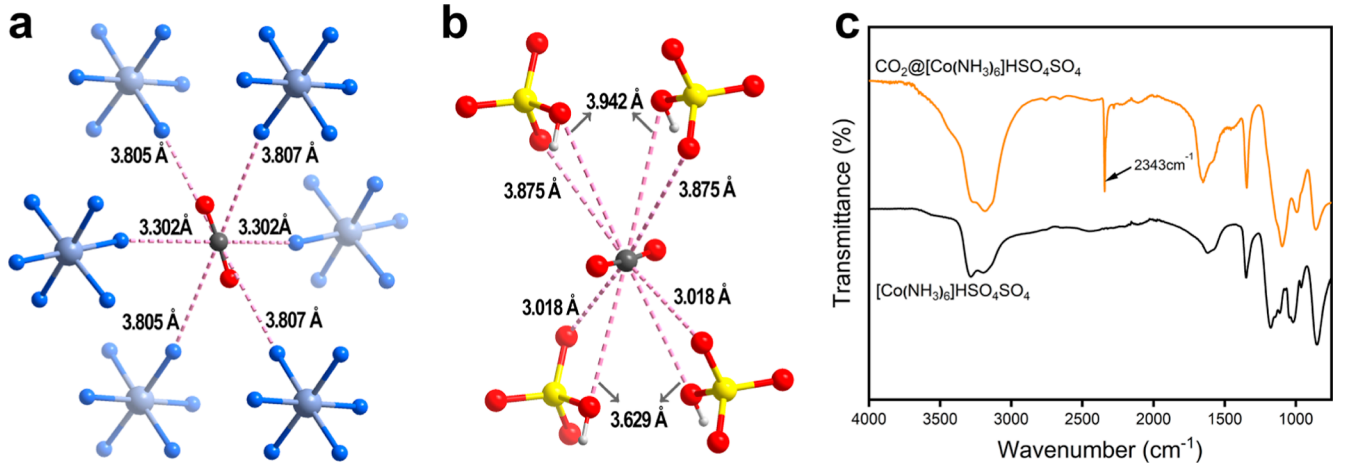

Figure 2. CO_2 interaction with CHAS motifs. Distances between CO_2 molecules and adjacent (a) $[Co(NH_3)_6]^{3+}$ ions and (b) HSO_4^-/SO_4^{2-} ions. (c) FTIR spectra of CHAS and CO_2@CHAS.

crystallizes in an orthorhombic system with the $P2_12_12$ space group, in which each $[Co(NH_3)_6]^{3+}$ ion contacts eight HSO_4^-/SO_4^{2-} ions, while one HSO_4^-/SO_4^{2-} ion connects with four $[Co(NH_3)_6]^{3+}$ ions to form a tetrahedral group via hydrogen bonds (Figure 1b,c). The H-bond distances range from 2.978 to 3.198 Å, and the N−H···O angles vary from 144.94 to 174.96° (Figure S6 and Table S3). The extension of such H-bond networking in three dimensions gives rise to a 3D hydrogen-bonded network with the CO_2 molecules confined inside, as shown in Figure 1d. In spite of the CO_2 insertion, the H-bond modes and the structure of CO_2@CHAS are similar to CHAS (Figures 1 and S2, Table S1). As CHAS is adsorption-free toward CO_2 (also for N_2) (Figure S4) and the forming process of CO_2@CHAS clathrate is completed in aqueous solution, the CO_2 inclusion in CO_2@CHAS is clearly a thermokinetic-dominated process rather than a sorption process.

Closely looking into the structure, it is found that one CO_2 molecule is neighbored by eight HSO_4^-/SO_4^{2-} and six $[Co(NH_3)_6]^{3+}$ ions, and thus CO_2 is locked in the cage constructed via H-bonds among those ions, taking HSO_4^-/SO_4^{2-} and six $[Co(NH_3)_6]^{3+}$ ions as vertexes (Figure 1e). For simplicity and clarification, directly connecting the adjacent S and Co generated a disordered granatohedron cage, and the stacking cage resulted in a 3D network with a flu topological structure (Figure 1f).[23] This granatohedron cage has a spherical cavity with a diameter of 3.4 Å and a volume of 20.57 $Å^3$ (Figures 1e and S2e), accommodating one CO_2 molecule inside (dynamic diameter of CO_2: 3.3 Å). A body-centered cubic zeolite-like hydrogen-bonded framework with supramolecular Archimedean cages assembled with 72 hydrogen bonds from tris(guanidinium)nitrate clusters and hexa(4-sulfonatophenyl)benzene ions has been reported and exhibited the ability to encapsulate a wide range of ionic guest species.[24] In contrast, most hydrogen-bonded organic frameworks (HOFs) assembled from neutral organic molecules of plane configuration generate a channel rather than a cage structure.[25]

The distances between C atoms with partially positive charges in CO_2 and $HSO_4^-/SO_4^{2-}/[Co(NH_3)_6]^{3+}$ ions (shortest atom distance) range from 3.018 to 3.942 Å (Figure 2a,b); however, no H-bonds are assigned because of the unfavorable N(O)−H···O angles (Figure S7). Therefore, CO_2 interacts with HSO_4^-/SO_4^{2-} and $[Co(NH_3)_6]^{3+}$ ions via electrostatic interactions rather than H-bonding or chemical bonding. We observed a typical peak at 2343 cm^{-1} resulting from the free CO_2 stretching vibration in the IR spectra (Figure 2c), which is consistent with the physisorbed CO_2 in porous materials and further proves the weak interaction between CO_2 and CHAS components in CO_2@CHAS.[26] The other peaks match well with the vibrations from CHAS. All the results indicate that there are multiple weak interactions, including H-bonds, electrostatic interactions, and van der Waals forces, among the three motifs in CO_2@CHAS, and these massive weak interactions work together as the driving force for CO_2 in situ inducing crystallization of CO_2@CHAS from aqueous solution. We show clear and convincing evidence that Co(III) coordination with NH_3 is effective in modulating NH_3−CO_2 electrostatic interactions instead of chemical reactions.

CO_2 Uptake Capacity. CO_2 is assembled in CO_2@CHAS crystals under near-ambient conditions with two CO_2 molecules accommodated in each unit cell with a volume of 671 $Å^3$, corresponding to a CO_2 volume density of 0.218 g·cm^{-3}. This is equal to approximately 121 m^3 of CO_2 in one cubic meter of CO_2@CHAS under ambient conditions. For comparison, an ordinary CO_2 cylinder stores 0.04 m^3 of CO_2 with a total weight of 10 kg and a pressure of 14 MPa at room temperature, corresponding to a volume density of 0.25 g·cm^{-3}. In terms of weight density, the CO_2 weight content in CO_2@CHAS is calculated to be 11.7 wt %. In industry, taking a typical adsorbent of MEA aqueous solution as an example, MEA of 30 wt % concentration in water adsorbs 2.1−5.5 wt % CO_2 depending on the CO_2 pressure and temperature.[27]

CO_2 clathrates in various host materials, including CO_2 hydrate, have been reported, as summarized in Table S4, which are generally formed under high-pressure conditions and/or low temperatures and exhibit moderate CO_2 uptake capacity.[28−32] Nevertheless, the harsh formation condition renders these clathrates infeasible for flue gas treatment in practice because deviation from ambient temperature and pressure always requires intensive energy input. Porous materials with ultrahigh specific surface areas usually give rise to high CO_2 uptake owing to their high surface energy and large pore volume.[33] For comparison, we list the CO_2 storage capacity of typical porous materials in Table S5. However, the poor stability, low selectivity, high cost, etc., restrict the

https://doi.org/10.1021/acsami.3c11994
ACS Appl. Mater. Interfaces 2023, 15, 54458−54465

practical application of porous materials at present. Therefore, CHAS shows comprehensive advantages for CO_2 capture in terms of adsorption amount, selectivity (especially from water), energy and material cost, and cycling performance.

Formation Conditions of CO_2@CHAS. We take the CO_2 pressure, temperature, and CHAS concentration into consideration to explore the formation conditions of CO_2@CHAS. It is found that higher pressure leads to a higher yield of CO_2@CHAS (Figure S8). To demonstrate the boundary condition for CO_2 assembling in CHAS and crystallizing CO_2@CHAS, we used a saturated solution with excess CHAS solid to investigate the temperature−pressure relationship of the CO_2−CHAS solution-precipitate system under the phase equilibrium state. As shown in Figure 3, the formation of CO_2@CHAS can

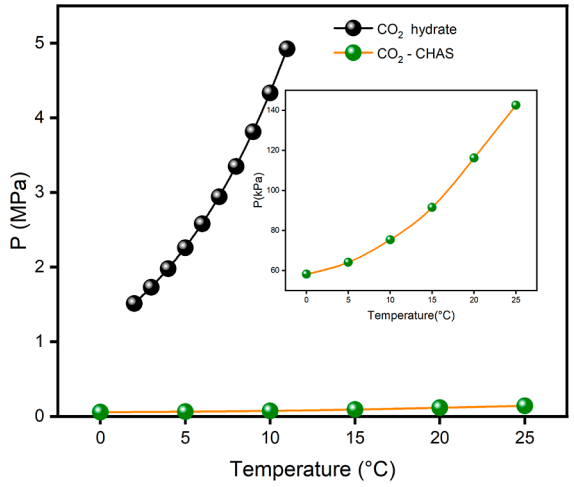

Figure 3. Phase diagram of the CO_2−CHAS system. Pressure−temperature correlations of the CO_2−CHAS aqueous system and the CO_2-water system under equilibrium. The inset shows the zoomed-in curves of the CO_2−CHAS system.

be completed under mild conditions in terms of the temperature and the CO_2 pressure. The temperature−pressure diagram of CO_2 hydrate (CO_2@H_2O_n) is given for reference, where the CO_2 hydrate formation at 275 K requires a CO_2 pressure up to 1500 kPa.[28] In sharp contrast, CO_2@CHAS crystallizes under 56 and 142 kPa of CO_2 at 275 and 298 K, respectively (Figure 3). The diagram is well fitted to the Clapeyron−Clausius equation; hence, we are able to calculate the enthalpy change of the assembling process (28.0 kJ/mol, Figures S9−S11). The value is comparable with the enthalpy changes in most CO_2 physisorption systems but much smaller than that in typical CO_2 chemisorption processes (>40 kJ/mol), which indicates the low energy consumption for CO_2 capture and release in such supramolecular processes.[34−36] Specifically, the enthalpy change of CO_2@CHAS formation/decomposition is only approximately half that of CO_2 hydrates (57.1 kJ/mol), as the decomposition of CO_2 hydrates breaks massive hydrogen bonds among H_2O molecules.[29]

Selectivity and Stability of CHAS. We designed an isochoric experiment to further illustrate the CO_2 capture process by monitoring the pressure change during the formation of CO_2@CHAS and its selective capture of CO_2 over nitrogen and water (the main components in flue gas). The autoclave containing a saturated CHAS solution and excess CHAS solid was charged with CO_2 to 1000 kPa at 293 K under constant stirring. The pressure dropped over time is monitored, which is ascribed to the formation of CO_2@CHAS (Figure 4a). When replacing the CHAS solution with the same volume of water, the CO_2 pressure drop is much decreased and becomes stable rapidly owing to the solubility of CO_2 in water (Figure 4a). The same experiment was performed on the N_2−CHAS solution system, and the result showed a negligible N_2 pressure drop, indicating that N_2 is not adsorbed (assembled) in the CHAS solution. The results show that CHAS exhibits a high selectivity for CO_2 capture over N_2 (Figure 4a). On the other hand, the assembly process is conducted in an aqueous solution, and there is no water included in the CO_2@CHAS, demonstrating the CO_2 selectivity over water.

To test the recyclability of the CO_2 uptake in CHAS, we cycled the CO_2 uptake and release process five times. After the pressure stabilized and the clathrate process reached an equilibrium state at 273 K, we warmed the autoclave to 303 K and found that the pressure recovered efficiently, which corresponds to the collapse of the CO_2@CHAS structure and the CO_2 release (Figure 4b). The result indicates a good cycling performance. Powder X-ray diffraction (PXRD) measurements confirmed that CHAS remained intact after cycling experiments (Figure 4c). Thermogravimetric analysis (TGA) revealed a discrepant decomposition behavior for the CHAS and CO_2@CHAS samples (Figures 4d and S12). We note a small weight loss between 100 and 150 °C for CO_2@CHAS, which might be from surface-adsorbed water. Another weight loss of 26.1% is marked between 150 and 270 °C, caused by the removal of NH_3 and CO_2 molecules (11.7 wt % of CO_2 in CO_2@CHAS theoretically). We collected the corresponding residue and recrystallized it in water, and the PXRD of the powder matched well with the $(NH_4)_2[Co(H_2O)_6](SO_4)_2$ phase (Figures 4d and S12). This result indicates that CO_2@CHAS lost one CO_2 and four NH_3 molecules at this stage, corresponding to a theoretical weight loss of 28.2% that agrees with the experimental value. Continuously increasing the temperature leads to another two NH_3 molecules leaving, and the final residue is identified to be the $CoSO_4$ phase (Figure S12a). For comparison, CHAS can survive up to >200 °C without weight loss, suggesting the good thermostability of CHAS (Figure S12). PXRD revealed that the $CoSO_4$ phase was formed after CHAS was heated at 700 °C for 2 h in an inert atmosphere (Figure S12a). It is believed that Co^{3+} is reduced into Co^{2+} by the decomposed NH_3. The residue weight of 43.3 wt % agrees well with the theoretical value of 43.7% (Figure S12c).

CO_2 Release. The crystals of CO_2@CHAS as precipitates are easily separated from the reaction solution by simply filtering or centrifugation. Different from the violent decomposition in water, the dry CO_2@CHAS crystals exhibit a sluggish decomposition process in an ambient atmosphere. The decomposition process is monitored by PXRD, in which it can be seen that CO_2@CHAS is not completely converted into CHAS in 2 h under an ambient atmosphere, even under grinding (Figure S13). The TGA curve of CO_2@CHAS also reveals that CO_2 will not be easily released in the ambient atmosphere (Figure 4d). We reasoned that the CO_2 release proceeded outside, and the dense CHAS formed on the surface after the escape of CO_2 blocked further CO_2 release from CO_2@CHAS. This process was greatly accelerated with the assistance of water owing to the dissolution of the generated CHAS on the surface (Video S1). In either situation, the obtained CHAS solid or solution could be directly used to perform another round of CO_2 capture without further

https://doi.org/10.1021/acsami.3c11994
ACS Appl. Mater. Interfaces 2023, 15, 54458−54465

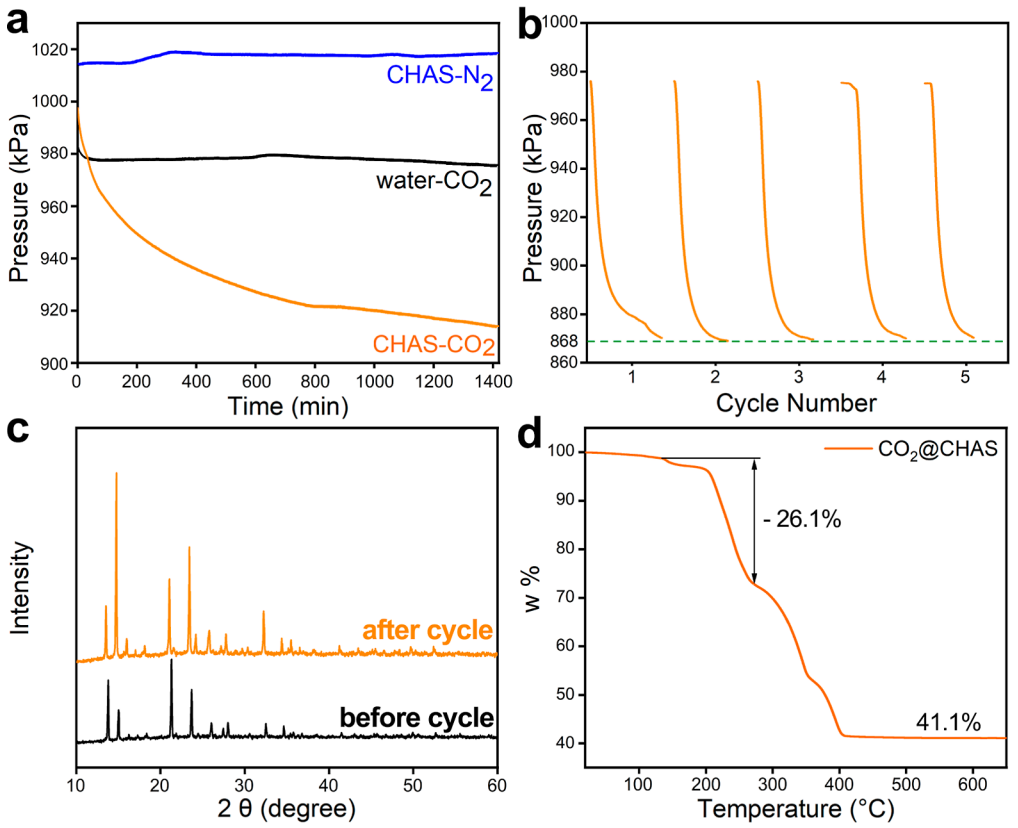

Figure 4. Selectivity and stability of CHAS over that of CO_2 capture. (a) CO_2 pressure change in the isochoric CO_2 sorption experiments. Controlling variables was done by replacing CO_2 with N_2 or changing the CHAS solution to pure water. (b) Cycling performance of CO_2 sorption in CHAS aqueous solution. (c) PXRD of CHAS before and after CO_2 capture experiments. (d) TGA curve of CO_2@CHAS in an inert atmosphere.

treatment. The CO_2 gathered through the release of CO_2@CHAS is 100% pure except for water vapor, which can be directly used in many fields, such as extinguisher use, gaseous fertilizer, scientific research studies, etc.

CONCLUSIONS

The hydrogen-bonded ionic framework of CHAS comprising massive H-bonds is nonporous as it exhibits no adsorption toward N_2 and CO_2. Although a cage structure is identified in the CHAS structure, the opening is too small to be accessed. Therefore, the carbon capture process is essentially different from a typical physisorption process. In contrast to chemisorption, there is no new chemical bond formation, so intensive energy input is not required for CHAS sorbent regeneration. CO_2@CHAS solid does not release CO_2 before 120 °C, owing to the resulting dense CHAS on the surface; nevertheless, the release of CO_2 via dissolution in water makes the process even easier and more energy-efficient. CHAS achieves reversible CO_2 capture/release via a clathrate-crystallization-dissolving (CCD) process at mild conditions and in an energy-efficient fashion. Capture is executed in an aqueous solution via assembling as a supramolecular reaction under ambient conditions; the product as a precipitate is spontaneously separated from the solution; the release is completed via dissolving; and the resulting CHAS aqueous solution is readily used for the next capture cycles.

Such a CCD process is conducted in an aqueous solution and displays exclusive selectivity for CO_2 (against the main components of flue gas: H_2O and N_2), which is compatible with the state-of-the-art MEA carbon capture technology in industry but greatly reduces the energy penalty for sorbent recycling. Meanwhile, the CCD process presented here is free from water or moisture interference, essentially overcoming the fatal weakness from any physisorption process. Associated with other advantages, such as cheap raw materials, low corrosivity, long durability, etc., the CCD process using CHAS as a sorbent shows great advance for carbon capture in practice. The test at the pilot scale is ongoing for a comprehensive evaluation of the cost advantage.

MATERIALS AND METHODS

Statement. No unexpected or unusually high safety hazards were encountered.

Materials and Instrumentation. All reagents and solvents were purchased from commercial sources. PXRD measurements were carried out on a Rigaku MiniFlex 600 X-ray diffractometer using Cu Kα radiation (λ = 1.54178 Å). The FTIR spectrum was measured by a Nicolet iS5 spectrophotometer with an attenuated total reflectance (ATR) module (Thermo Fisher Scientific, USA). The X-ray photoelectron spectrum was recorded on an ESCA Lab MKII XPS instrument using an Mg Ka radiation source. TGA techniques were performed from 25 to 700 °C at a heating rate of 5 °C/min in a N_2 atmosphere on a TGA Q500 integration thermal analyzer.

Single-Crystal X-ray Crystallography. SCXRD data of $[Co(NH_3)_6][HSO_4][SO_4]$ and CO_2@$[Co(NH_3)_6][HSO_4][SO_4]$ were collected on a Rigaku Oxford Diffraction diffractometer with Cu Kα radiation at 298 and 100 K, respectively. Empirical absorption corrections were applied using the SADABS program (Bruker AXS Inc., Madison, Wisconsin, USA). The structures were solved by direct methods and refined by the full matrix least-squares method based on F2 using the SHELXTL 14XL program package. For CO_2@$[Co(NH_3)_6][HSO_4][SO_4]$, the maximum electron density is high owing

https://doi.org/10.1021/acsami.3c11994
ACS Appl. Mater. Interfaces 2023, 15, 54458−54465

to the effects of series-termination errors in the Fourier syntheses. Hydrogen atom positions were calculated geometrically and refined by using the riding model. Full details of the structural analyses are summarized in Table S1. Hydrogen-bonding lengths (Å) and angles (deg) are given in Tables S2 and S3, respectively.

Synthesis of CHAS. $CoSO_4{\cdot}7H_2O$ (22.4 g, 0.08 mol) was dissolved in water (100 mL), and activated charcoal (1.5 g) was added as a catalyst. After stirring for 10 min, $NH_3{\cdot}H_2O$ (60 mL, 28%, 0.8 mol) was poured into the solution quickly with constant stirring. Hydrogen peroxide (40 mL, 30%, 0.4 mol) was slowly added to the system above, and then the solution was heated with stirring for 20 min. After that, the mixture was filtered to get a clear solution, concentrated H_2SO_4 (20 mL, 98%, 0.37 mol) was added to the solution, and the mixture was stirred for homogeneous dispersion. After that, MeOH (100 mL) was added to the solution, the precipitation was collected through centrifugation, and it was washed with abundant MeOH to get the crude product (22.1 g, 78.0% yield). The crude product was dried and then recrystallized in 50 mL of ultrapure water for purification. The refined product was collected by filtration, dried, and weighted (15.6 g, 55.1% yield). PXRD was used to verify the phase purity of the product. XPS was used to clarify the valence state of the Co species in CHAS (Figure S1).

Synthesis of CO_2@CHAS Single Crystals. CHAS (1.118 g) was dissolved in water (10 mL), and the solution was placed in a glass vial that was placed in an autoclave. The air in the autoclave was removed by CO_2 flushing three times. Finally, the autoclave is charged with CO_2 at 2 MPa. The temperature of the autoclave was controlled at 0 °C by using a cooling jacket. Orange crystals were obtained after 12 h.

Pressure Effect on Conversion of CHAS. CHAS aqueous solution was added to a glass vial and weighed together. The vial was put into an autoclave connected to the CO_2 cylinder, and the air in the autoclave was exchanged with CO_2 three times. Then, the CO_2 pressure inside the autoclave was controlled at the set value. The temperature of the autoclave was controlled at 0 °C using a cooling jacket. After the reaction for 12 h, the pressure was disclosed, and the vial containing CHAS aqueous solution was weighed again to calculate the conversion rate (Figure S7). Note: the dissolved CO_2 was ignored in the conversion calculation, as CO_2 dissolved in solution is negligible in comparison to that adsorbed by CHAS.

Measurement of Pressure−Temperature Correlation of the CO_2−CHAS Aqueous System under Equilibrium State. Saturated CHAS solution (25 mL) at 40 °C and excess CHAS powder (2.3 g) were added to a 60 mL autoclave under constant stirring. The temperature in the autoclave was controlled at 0 °C by using a cooling jacket. The gas in the autoclave was vacuumed to evacuate the air and flushed with CO_2. This procedure was repeated three times to ensure complete removal of the air in the autoclave. Then, the autoclave was charged with CO_2 at 200 kPa. We observed the pressure drop until it became unchanged via a digital pressure recorder (5 s per point). The final pressure was taken as the equilibrium pressure at the set temperature (0, 5, 10, 15, 20, and 25 °C) (Figure S8). The pressure of vapor from the solution of CHAS was measured through the same method but without CO_2 added in the autoclave (Figure S9). The water vapor pressure at the varied temperatures was subtracted to calculate the CO_2 equilibrium pressure−temperature correlation (Figure S10).

Cycling Capture/Release Experiment. The saturated CHAS solution (5 mL) was placed in a vial that was put into a 60 mL autoclave, and the temperature of the autoclave was controlled using a cooling jacket. We charged CO_2 to 2 MPa and released it three times to evacuate the air in the autoclave. Finally, the pressure in the autoclave was controlled at 1 MPa, and we used a digital pressure recorder (5 s per point) to monitor the pressure change while we switched the temperature from 0 to 30 °C and kept constant stirring. The procedures are repeated to test the cycling performance of CO_2 adsorption for five rounds. After the final round of cycling, we tested the PXRD of the precipitate recrystallized from the solution and found that it was consistent with that of CHAS.

Isochoric Sorption Experiment. The saturated CHAS solution (2 mL) and excess CHAS powder (0.6 g) were placed in a vial that was put into a 60 mL autoclave, and the temperature of the autoclave was controlled using a cooling jacket. We charged CO_2 to 2 MPa and released it three times to evacuate the air in the autoclave. Finally, the pressure in the autoclave was controlled at 1 MPa, and we used a digital pressure recorder (5 s per point) to record the change in pressure while the temperature was set at a constant 25 °C and kept constant stirring. We conducted control experiments by replacing the CHAS solution with pure water of the same volume or replacing CO_2 with N_2.

■ ASSOCIATED CONTENT

Supporting Information

The Supporting Information is available free of charge at https://pubs.acs.org/doi/10.1021/acsami.3c11994.

Experimental details; scheme for related reaction formulas; results of PXRD, TGA, XPS, and BET; tables of crystal data and structure determination for $[Co(NH_3)_6][HSO_4][SO_4]$ and CO_2@$[Co(NH_3)_6][HSO_4][SO_4]$; and table of similar compounds (PDF)

CO_2 release from CO_2@CHAS in water at room temperature (MP4)

CHAS (CIF)

CO_2-CHAS(CIF)

■ AUTHOR INFORMATION

Corresponding Authors

Cafer. T. Yavuz − *Oxide & Organic Nanomaterials for Energy & Environment (ONE) Laboratory, Chemistry Program, Advanced Membranes & Porous Materials (AMPM) Center, KAUST Catalysis Center (KCC), Physical Science & Engineering (PSE), King Abdullah University of Science and Technology (KAUST), Thuwal 23955, Saudi Arabia;* orcid.org/0000-0003-0580-3331; Email: cafer.yavuz@kaust.edu.sa

Qiang Xu − *Shenzhen Key Laboratory of Micro/Nano-Porous Functional Materials (SKLPM), SUSTech-Kyoto University Advanced Energy Materials Joint Innovation Laboratory (SKAEM-JIL), Department of Chemistry, and Department of Materials Science and Engineering, Southern University of Science and Technology (SUSTech), Shenzhen 518055, P. R. China; Institute for Integrated Cell-Material Sciences (iCeMS), Kyoto University, Kyoto 606-8501, Japan;* orcid.org/0000-0001-5385-9650; Email: xuq@sustech.edu.cn, xu.qiang@icems.kyoto-u.ac.jp

Bo Liu − *School of Chemistry and Materials Science, University of Science and Technology of China, Hefei, Anhui 230026, P. R. China;* orcid.org/0000-0002-1150-3709; Email: liuchem@ustc.edu.cn

Authors

Xiao Lu − *School of Chemistry and Materials Science, University of Science and Technology of China, Hefei, Anhui 230026, P. R. China*

Congyan Liu − *School of Chemistry and Materials Science, University of Science and Technology of China, Hefei, Anhui 230026, P. R. China*

Xin Xiao − *Shenzhen Key Laboratory of Micro/Nano-Porous Functional Materials (SKLPM), SUSTech-Kyoto University Advanced Energy Materials Joint Innovation Laboratory (SKAEM-JIL), Department of Chemistry, and Department of Materials Science and Engineering, Southern University of Science and Technology (SUSTech), Shenzhen 518055, P. R. China*

Thien S. Nguyen − *Oxide & Organic Nanomaterials for Energy & Environment (ONE) Laboratory, Chemistry Program, Advanced Membranes & Porous Materials (AMPM) Center, KAUST Catalysis Center (KCC), Physical Science & Engineering (PSE), King Abdullah University of Science and Technology (KAUST), Thuwal 23955, Saudi Arabia;* orcid.org/0000-0003-4286-0343

Zhiling Xiang − *School of Chemistry and Materials Science, University of Science and Technology of China, Hefei, Anhui 230026, P. R. China*

Chunhui Chen − *School of Chemistry and Materials Science, University of Science and Technology of China, Hefei, Anhui 230026, P. R. China*

Songlin Cui − *School of Chemistry and Materials Science, University of Science and Technology of China, Hefei, Anhui 230026, P. R. China*

Complete contact information is available at: https://pubs.acs.org/10.1021/acsami.3c11994

Author Contributions

B. L conceived of the idea, and B. L., Q. X., and C. T. Y. supervised the project together. X. L. designed and carried out the experiments. C. Y. L., Z.L. X., X. X., and T. S. N. contributed to data analysis and manuscript preparation. C.H. C. collected the SCXRD data and solved the structure. S.L. C. performed the gas sorption experiments. B. L., Q. X., and C. T. Y. wrote the manuscript together. All authors discussed the results and assisted with the manuscript preparation.

Funding

National Key Research and Development Program of China (2021YFA1500402), National Natural Science Foundation of China (NSFC, 21571167, 51502282, and 22075266), and Fundamental Research Funds for the Central Universities (WK2060190053 and WK2060190100).

Notes

The authors declare no competing financial interest.

■ ACKNOWLEDGMENTS

We acknowledge the support from the Chinese Academy of Sciences and University of Science and Technology of China and the King Abdullah University of Science and Technology (KAUST).

■ REFERENCES

(1) Wuebbles, D. J.; Jain, A. K. Concerns About Climate Change and the Role of Fossil Fuel Use. *Fuel Process. Technol.* **2001**, *71* (1−3), 99−119.

(2) Liu, Z.; Ciais, P.; Deng, Z.; Davis, S. J.; Zheng, B.; Wang, Y. L.; Cui, D.; Zhu, B. Q.; Dou, X. Y.; Ke, P. Y.; Sun, T. C.; Guo, R.; Zhong, H. W.; Boucher, O.; Breon, F. M.; Lu, C. X.; Guo, R. T.; Xue, J. J.; Boucher, E.; Tanaka, K.; Chevallier, F. Carbon Monitor, a Near-real-time Daily Dataset of Global CO_2 Emission from Fossil Fuel and Cement Production. *Sci. Data* **2020**, *7* (1), 392.

(3) Lai, J. Y.; Ngu, L. H.; Hashim, S. S. A Review of CO_2 Adsorbents Performance for Different Carbon Capture Technology Processes Conditions. *Greenhouse Gases: Sci. Technol.* **2021**, *11* (5), 1076−1117.

(4) Yu, C. H.; Huang, C. H.; Tan, C. S. A Review of CO_2 Capture by Absorption and Adsorption. *Aerosol Air Qual. Res.* **2012**, *12* (5), 745−769.

(5) Bottoms, R. J. U. P. Separating Acid Gases, Girdler Corp. 1930, U.S. patent 1783901 A.

(6) Gargiulo, N.; Pepe, F.; Caputo, D. CO_2 Adsorption by Functionalized Nanoporous Materials: a Review. *J. Nanosci. Nanotechnol.* **2014**, *14* (2), 1811−1822.

(7) Seipp, C. A.; Williams, N. J.; Kidder, M. K.; Custelcean, R. CO_2 Capture from Ambient Air by Crystallization with a Guanidine Sorbent. *Angew. Chem., Int. Ed.* **2017**, *56* (4), 1042−1045.

(8) Custelcean, R.; Garrabrant, K. A.; Agullo, P.; Williams, N. J. Direct Air Capture of CO_2 with Aqueous Peptides and Crystalline Guanidines. *Cell Rep. Phys. Sci.* **2021**, *2* (4), 100385.

(9) Luis, P. Use of Monoethanolamine (MEA) for CO_2 Capture in a Global Scenario: Consequences and Alternatives. *Desalination* **2016**, *380*, 93−99.

(10) Zhao, B. T.; Su, Y. X.; Tao, W. W.; Li, L. L.; Peng, Y. C. Postcombustion CO_2 Capture by Aqueous Ammonia: A State-of-the-art Review. *Int. J. Greenhouse Gas Control* **2012**, *9*, 355−371.

(11) Wang, F.; Deng, S.; Zhao, J.; Yan, J. A Novel Ammonia-based CO_2 Capture Process Hybrid Ammonia Absorption Refrigeration. *Energy Procedia* **2017**, *142*, 3734−3740.

(12) Yu, H.; Xiang, Q. Y.; Fang, M. X.; Yang, Q.; Feron, P. Promoted CO_2 Absorption in Aqueous Ammonia. *Greenhouse Gases: Sci. Technol.* **2012**, *2* (3), 200−208.

(13) Milani, D.; Yu, H.; Cottrell, A.; Yang, C. Y.; Maher, D.; Green, P.; Wardhaugh, L. Process Enhancement in Aqueous Ammonia PCC Using a Direct Contact Condenser. *Greenhouse Gases: Sci. Technol.* **2019**, *9* (2), 245−260.

(14) Fang, M.; Xiang, Q.; Zhou, X.; Ma, Q.; Luo, Z. Experimental Study on CO_2 Absorption into Aqueous Ammonia-based Blended Absorbents. *Energy Procedia* **2014**, *61*, 2284−2288.

(15) Wang, T.; Lackner, K. S.; Wright, A. Moisture Swing Sorbent for Carbon Dioxide Capture from Ambient Air. *Environ. Sci. Technol.* **2011**, *45* (15), 6670−6675.

(16) Choi, S.; Gray, M. L.; Jones, C. W. Amine-Tethered Solid Adsorbents Coupling High Adsorption Capacity and Regenerability for CO_2 Capture from Ambient Air. *ChemSusChem* **2011**, *4* (5), 628−635.

(17) Choi, S.; Drese, J. H.; Eisenberger, P. M.; Jones, C. W. Application of Amine-tethered Solid Sorbents for Direct CO_2 Capture from the Ambient Air. *Environ. Sci. Technol.* **2011**, *45* (6), 2420−2427.

(18) Gebald, C.; Wurzbacher, J. A.; Tingaut, P.; Zimmermann, T.; Steinfeld, A. Amine-based Nanofibrillated Cellulose as Adsorbent for CO_2 Capture from Air. *Environ. Sci. Technol.* **2011**, *45* (20), 9101−9108.

(19) Goeppert, A.; Czaun, M.; May, R. B.; Prakash, G. K. S.; Olah, G. A.; Narayanan, S. R. Carbon Dioxide Capture from the Air Using a Polyamine Based Regenerable Solid Adsorbent. *J. Am. Chem. Soc.* **2011**, *133* (50), 20164−20167.

(20) Ben-Mansour, R.; Habib, M. A.; Bamidele, O. E.; Basha, M.; Qasem, N. A. A.; Peedikakkal, A.; Laoui, T.; Ali, M. Carbon capture by physical adsorption: Materials, experimental investigations and numerical modeling and simulations − A review. *Appl. Energy* **2016**, *161*, 225−255.

(21) Xiang, Z.; Liu, C.; Chen, C.; Xiao, X.; Nguyen, T. S.; Yavuz, C. T.; Xu, Q.; Liu, B. Synthesis of Stable Single-crystalline Carbon Dioxide Clathrate Powder by Pressure Swing Crystallization. *Cell Rep. Phys. Sci.* **2023**, *4* (5), 101383.

(22) Wang, C. L.; Zhan, H. J.; Lu, X. H.; Jing, R.; Zhang, H. F.; Yang, L.; Li, X. X.; Yue, F. F.; Zhou, D.; Xia, Q. H. A Recyclable Cobalt(III)-ammonia Complex Catalyst for Catalytic Epoxidation of Olefins with Air as the Oxidant. *New J. Chem.* **2021**, *45* (4), 2147−2156.

(23) Delgado-Friedrichs, O.; O'Keeffe, M.; Yaghi, O. M. Three-periodic Nets and Tilings: Edge-transitive Binodal Structures. *Acta Crystallogr., Sect. A: Found. Crystallogr.* **2006**, *62*, 350−355.

(24) Liu, Y. Z.; Hu, C. H.; Comotti, A.; Ward, M. D. Supramolecular Archimedean Cages Assembled with 72 Hydrogen Bonds. *Science* **2011**, *333* (6041), 436−440.

(25) Lin, R. B.; Chen, B. L. Hydrogen-bonded Organic Frameworks: Chemistry and Functions. *Chem* **2022**, *8* (8), 2114−2135.

(26) Dong, X. L.; Ding, C. X.; Zhang, Q. N.; Chen, M. H.; Zhao, L. L.; Zhou, M. F.; Frenking, G. Covalent Bonding Between Be^+ and CO_2 in $BeOCO^+$ with a Surprisingly, High Antisymmetric OCO

Stretching Vibration. *J. Am. Chem. Soc.* **2021**, *143* (35), 14300−14305.
(27) Oyenekan, B. A.; Rochelle, G. T. Alternative Stripper Configurations for CO_2 Capture by Aqueous Amines. *AIChE J.* **2007**, *53* (12), 3144−3154.
(28) Sloan, E. D., Jr; Koh, C. A. *Clathrate Hydrates of Natural Gases*; CRC Press, 2007.
(29) Lee, Y.; Lee, S.; Lee, J.; Seo, Y. Structure Identification and Dissociation Enthalpy Measurements of the CO_2+N_2 Hydrates for Their Application to CO_2 Capture and Storage. *Chem. Eng. J.* **2014**, *246*, 20−26.
(30) Hashimoto, S.; Murayama, S.; Sugahara, T.; Ohgaki, K. Phase Equilibria for H_2+CO_2 + tetrahydrofuran+water Mixtures Containing Gas Hydrates. *J. Chem. Eng. Data* **2006**, *51* (5), 1884−1886.
(31) Lee, S.; Park, S.; Lee, Y.; Lee, J.; Lee, H.; Seo, Y. Guest Gas Enclathration in Semiclathrates of Tetra-n-butylammonium Bromide: Stability Condition and Spectroscopic Analysis. *Langmuir* **2011**, *27* (17), 10597−10603.
(32) Torre, J. P.; Coupan, R.; Chabod, M.; Pere, E.; Labat, S.; Khoukh, A.; Brown, R.; Sotiropoulos, J. M.; Gornitzka, H. CO_2-Hydroquinone Clathrate: Synthesis, Purification, Characterization and Crystal Structure. *Cryst. Growth Des.* **2016**, *16* (9), 5330−5338.
(33) Singh, G.; Lee, J.; Karakoti, A.; Bahadur, R.; Yi, J. B.; Zhao, D. Y.; AlBahily, K.; Vinu, A. Emerging Trends in Porous Materials for CO_2 Capture and Conversion. *Chem. Soc. Rev.* **2020**, *49* (13), 4360−4404.
(34) Gurkan, B. E.; de la Fuente, J. C.; Mindrup, E. M.; Ficke, L. E.; Goodrich, B. F.; Price, E. A.; Schneider, W. F.; Brennecke, J. F. Equimolar CO_2 Absorption by Anion-Functionalized Ionic Liquids. *J. Am. Chem. Soc.* **2010**, *132* (7), 2116−2117.
(35) Caskey, S. R.; Wong-Foy, A. G.; Matzger, A. J. Dramatic Tuning of Carbon Dioxide Uptake via Metal Substitution in a Coordination Polymer with Cylindrical Pores. *J. Am. Chem. Soc.* **2008**, *130* (33), 10870−10871.
(36) Cavenati, S.; Grande, C. A.; Rodrigues, A. E. Adsorption Equilibrium of Methane, Carbon Dioxide, and Nitrogen on Zeolite 13X at High Pressures. *J. Chem. Eng. Data* **2004**, *49* (4), 1095−1101.

https://doi.org/10.1021/acsami.3c11994
ACS Appl. Mater. Interfaces 2023, 15, 54458−54465